

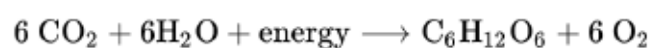
Atmospheric chemistry and aerosols (I)

Composition of planetary atmospheres

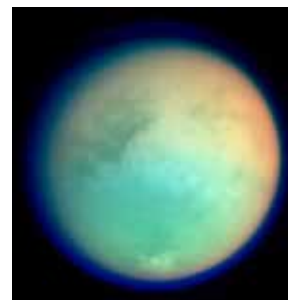
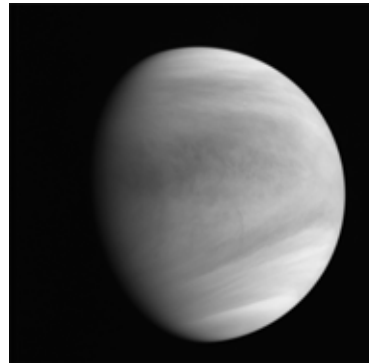
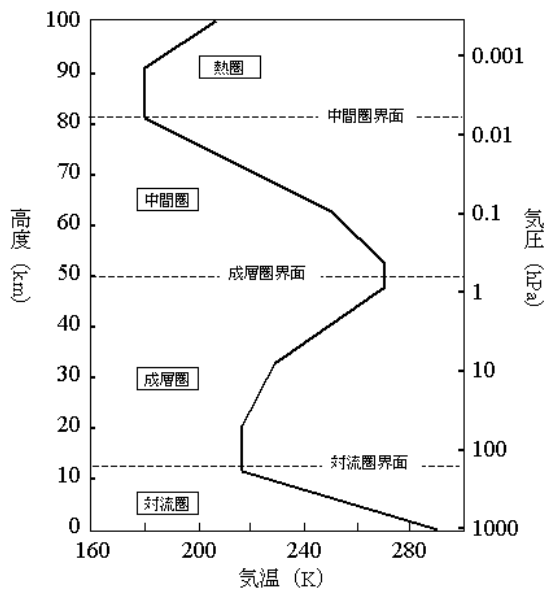
| Object | Mass (kilograms) | Carbon Dioxide | Nitrogen | Oxygen | Argon | Methane | Sodium | Hydrogen | Helium | Other |
|---------|----------------------|----------------|----------|--------|-------|---------|--------|----------|--------|-------|
| Sun | 3.0×10^{30} | | | | | | | 71% | 26% | 3% |
| Mercury | 1000 | | | 42% | | | 22% | 22% | 6% | 8% |
| Venus | 4.8×10^{20} | 96% | 4% | | | | | | | |
| Earth | 1.4×10^{21} | | 78% | 21% | 1% | | | | | <1% |
| Moon | 100,000 | | | | 70% | | 1% | | 29% | |
| Mars | 2.5×10^{16} | 95% | 2.7% | | 1.6% | | | | | 0.7% |
| Jupiter | 1.9×10^{27} | | | | | | | 89.8% | 10.2% | |
| Saturn | 5.4×10^{26} | | | | | | | 96.3% | 3.2% | 0.5% |
| Titan | 9.1×10^{18} | | 97% | | | 2% | | | | 1% |
| Uranus | 8.6×10^{25} | | | | | 2.3% | | 82.5% | 15.2% | |
| Neptune | 1.0×10^{26} | | | | | 1.0% | | 80% | 19% | |
| Pluto | 1.3×10^{14} | 8% | 90% | | | 2% | | | | |

from NASA HP

photosynthesis



Need for understanding chemistry



Chemical kinetics

A reaction between reactants A and B to form product C:



$$\text{reaction rate} = k [A] [B]$$



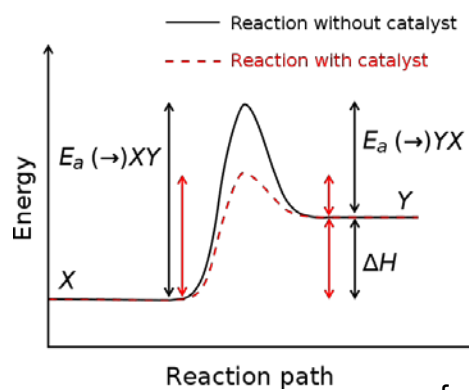
$$\text{reaction rate} = k [A] [B] [M]$$

M is any inert molecule that can remove the excess energy.

k is the reaction rate constant that usually depends on the temperature as (Arrhenius equation):

$$k = A \exp\left(-\frac{E_a}{k_B T}\right)$$

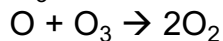
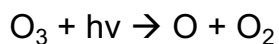
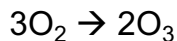
where E_a is the activation energy.



from Wikipedia

Production and destruction of ozone

Chapman theory



- Chapman theory predicts an ozone amount of several times larger than the observations.
- Other loss mechanisms are required.

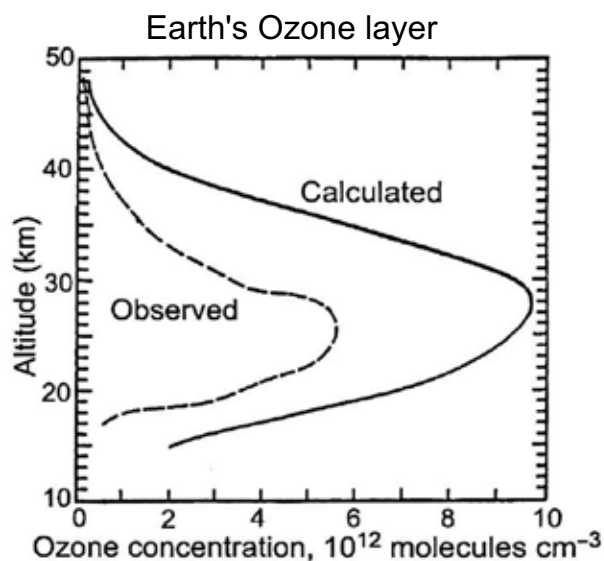
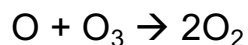
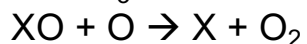
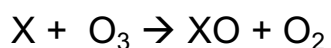


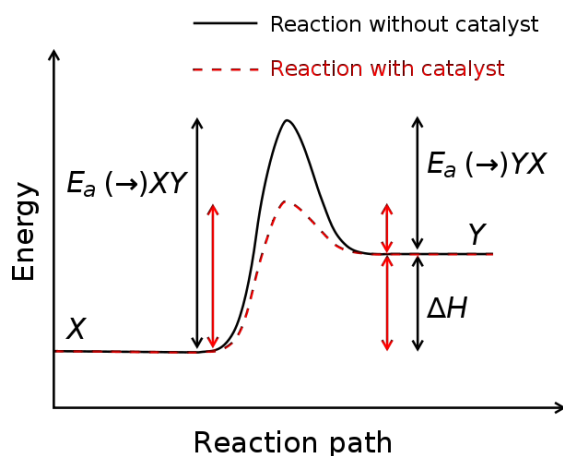
Figure 3.1 An ozone profile calculated with the Chapman reactions at the equator overestimates the ozone compared with observations over Panama at 9° N on November 13, 1970. The reason is that natural catalysts that destroy ozone are omitted from the oxygen-only Chapman reactions. (Adapted from Seinfeld and Pandis (1998). Reproduced with permission. Copyright 1998, John Wiley and Sons.)

Catling & Kasting (2017)

Catalytic cycles

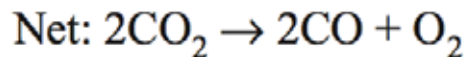
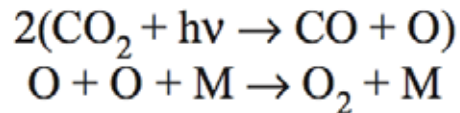


X : Free radical such as OH, NO, Cl, Br



The net result of the catalytic cycle is to remove O and O₃ rapidly.

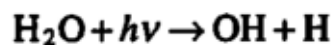
Stability of CO₂ atmosphere



The reaction $\text{CO} + \text{O} \rightarrow \text{CO}_2$ is very slow (spin forbidden).
Mars and Venus atmospheres are expected to be converted to CO and O₂ in 6000 years.

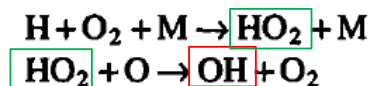
Catalytic cycle on Mars ?

On Mars, OH radicals are thought to play crucial roles.



McElroy and Donahue [1972]

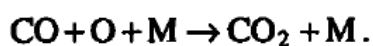
Production of OH



Production of CO₂

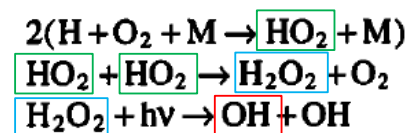


Net reaction

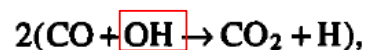


Parkinson and Hunten [1972]

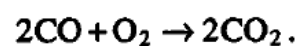
Production of OH



Production of CO₂



Net reaction



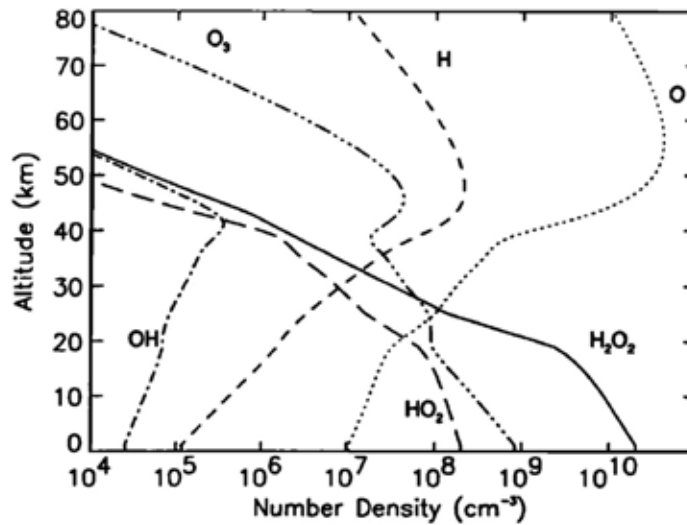
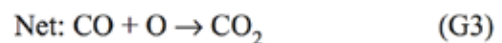
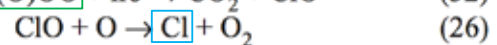
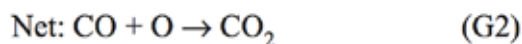
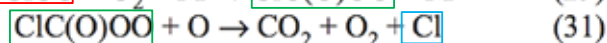
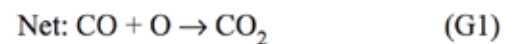
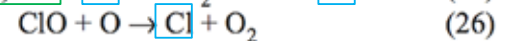
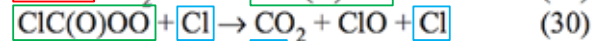
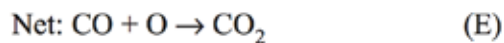
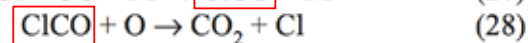


Figure 8. Distribution of key constituents based on the nominal model ($H_2O = 150$ ppm, $K = 10^6 \text{ cm}^2 \text{ s}^{-1}$, $\tau_d = 0.4$; see text).

Photochemistry is effective even near the surface on Mars because of the thin atmosphere.

Catalytic cycle on Venus?

Cl radicals are thought to play crucial roles.



Mills et al. (2007)

Vega-2 X-ray spectrometer result
(Andreychikov et al. 1987)

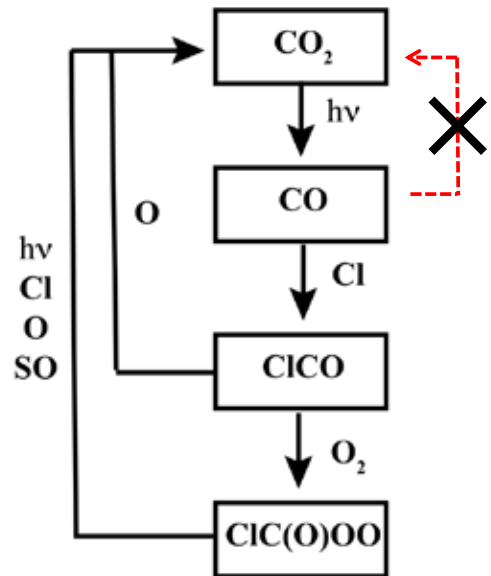
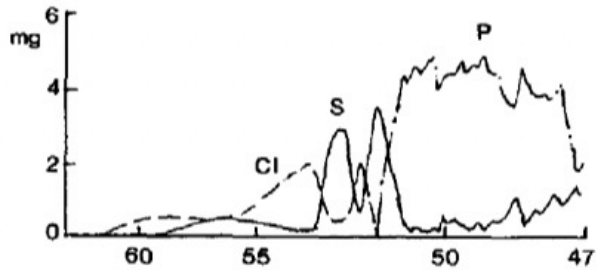
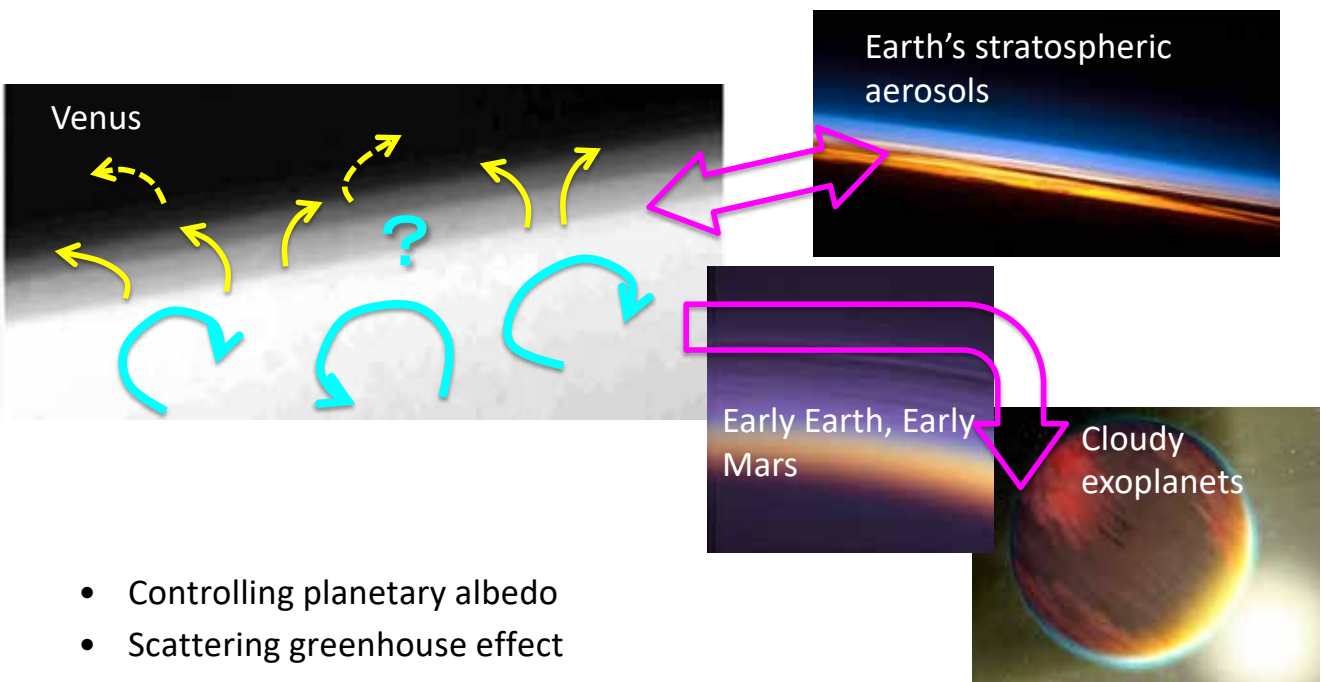


Figure 3. Schematic showing primary pathways for production of CO₂ via chlorine chemistry. The reaction ClCO + O → CO₂ + Cl accounts for 15 and 20% of the column total CO₂ production in the +0.5σ and +2.0σ models from Table 5, respectively.

ClCO, ClCO₃ and other key species have never been observed.

Clouds/aerosols



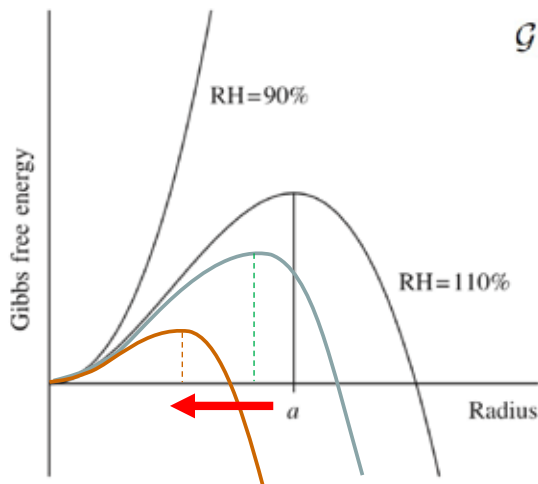
- Controlling planetary albedo
- Scattering greenhouse effect
- Regulating atmospheric species transported to the upper atmosphere

Cloud formation

Andrews (2010)

Gibbs free energy

$$\mathcal{G} - \mathcal{G}_0 = -\frac{4}{3}\pi a^3 \rho_l R_v T \ln\left(\frac{e}{e_s(T)}\right) + 4\pi a^2 \gamma$$



- a : radius of droplet
- e : partial vapor pressure
- e_s : saturation vapor pressure
- γ : surface tension
- ρ_l : liquid density
- R_v : gas constant
- T : temperature

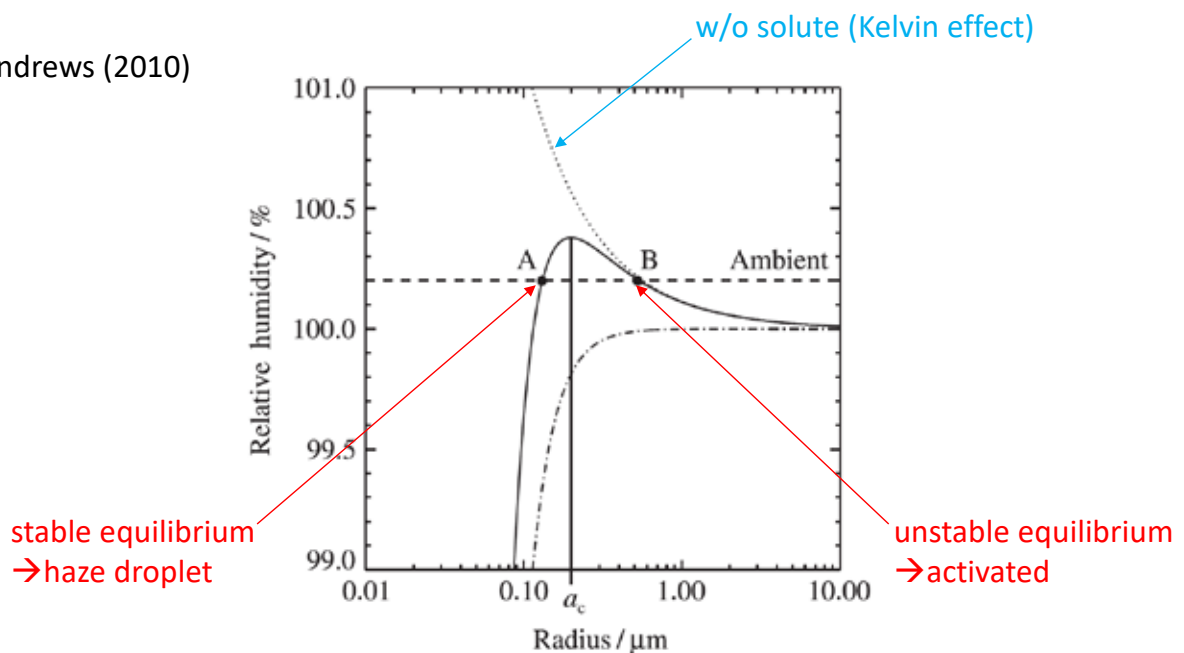
Pure water:

| equilibrium radius | relative humidity(RH) |
|--------------------|-----------------------|
| 0.01 μm | \rightarrow 112% |
| 0.1 μm | \rightarrow 101% |
| flat surface | \rightarrow 100% |

If a cloud droplet is to survive, it must somehow attain a radius greater than the equilibrium radius a corresponding to the ambient relative humidity
 \rightarrow Need for condensation nucleus

Role of soluble cloud condensation nuclei (CCN)

Andrews (2010)



The Köhler curve (solid) for the relative humidity $RH = e/e_s$ over a spherical droplet of water containing solute, as a function of droplet radius a , at 5 °C. The solute is taken to be 10^{-19} kg of NaCl. The Kelvin factor is given by the dotted curve and the Raoult factor is given by the dash-dotted curve. The thick horizontal dashed line and points A and B are discussed in the text.

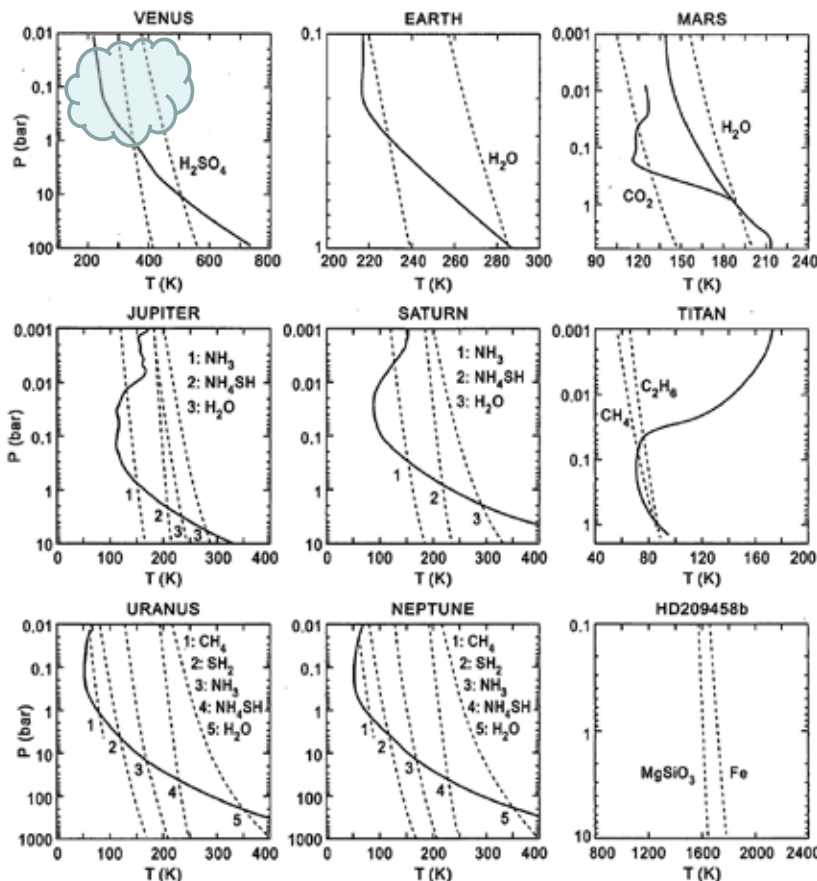
Composition of CCN

Example of the composition of ice forming nuclei in Earth's troposphere (Pruppacher & Klett 1997)

TABLE 9.6
Composition of ice forming nuclei derived from aerosolized soil in Montana (from Rosinski *et al.*, 1981).

| Chemical composition | Aerosol particles | | Ice-forming nuclei active at temperature | | | | | |
|-------------------------------------|-------------------|----|--|----|--------|----|--------|----|
| | number | % | number | % | number | % | number | % |
| Clay minerals: | | | | | | | | |
| montmorillonite | 194 | 24 | 28 | 18 | 17 | 13 | 41 | 28 |
| feldspar | 287 | 36 | 74 | 48 | 41 | 32 | 54 | 38 |
| illite | 163 | 20 | 37 | 24 | 39 | 31 | 28 | 19 |
| miscellaneous | 27 | 3 | 8 | 5 | 19 | 15 | 10 | 7 |
| Organic particles | 139 | 17 | 7 | 5 | 12 | 9 | 11 | 8 |
| Number of particles: analyzed | 810 | | 154 | | 128 | | 144 | |
| Mixed particles containing: | | | | | | | | |
| NaCl | 7 | | 14 | 9 | 28 | 22 | 21 | 15 |
| CuX | 2 | | 1 | | 0 | | 1 | |
| Fe _{0x} ·nH ₂ O | - | | 7 | 5 | 12 | 9 | 11 | 8 |
| Total | 9 | | 22 | 14 | 40 | 31 | 33 | 23 |

- The characteristics of CCN on other planets are totally unknown.
- Dust particles will serve as CCN on Mars.
- Galactic cosmic rays may also work. Cosmic rays increase small ions (charged molecules or charged small clusters of molecules) in the atmosphere, leading to increase in the nucleation rate of aerosol particles.

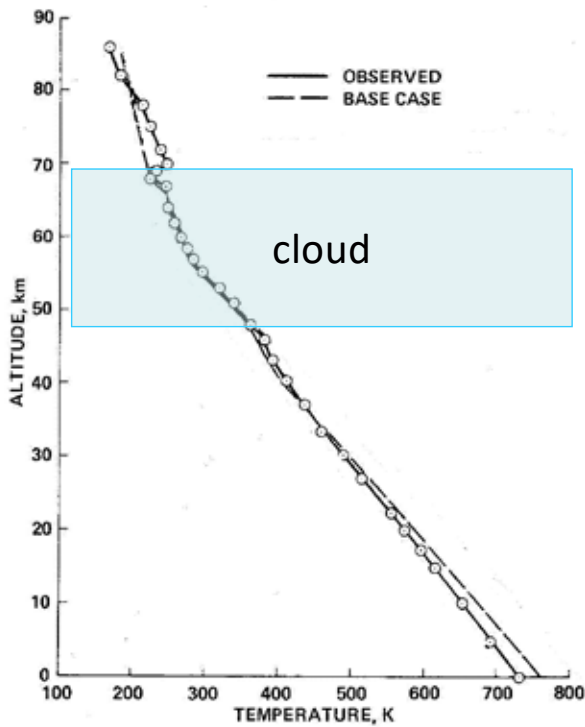


Catling & Kasting (2017)

The solid curves are the typical vertical profiles of pressure versus temperature. Dashed curves are the saturation vapor pressure curves for various condensables.

Particles condense when the partial pressure reaches the saturation vapor pressure.

H₂SO₄ clouds of Venus

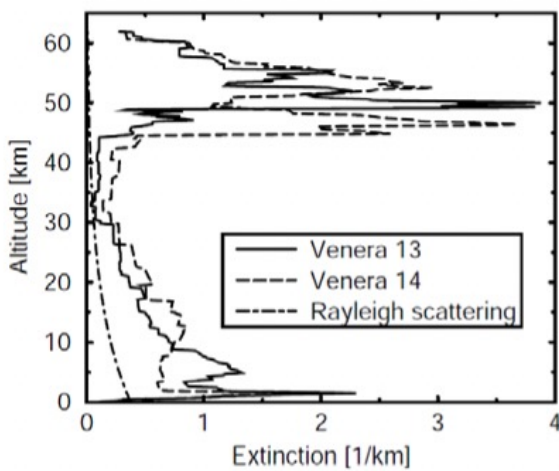


- Solar energy flux reaching the Venus surface (17W/m²) is much less than that of the Earth (168W/m²).
- Greenhouse effect of massive CO₂ and small amount of H₂O explains the high temperature.

Fig. 2. Comparison between the observed temperature structure of Venus' lower atmosphere and that of several models, which are described in the main text.

Pollack et al. (1980)

Extinction profiles as retrieved from Venera 13 & 14 spectrophotometer data at 700-710 nm (Grieger et al. 2003)



Tomasko et al. (1980)

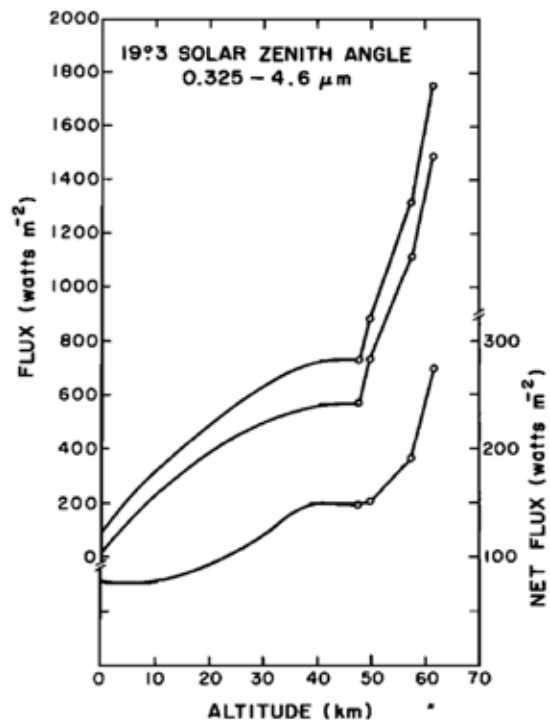
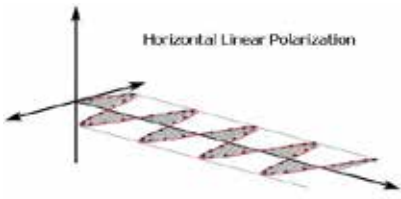
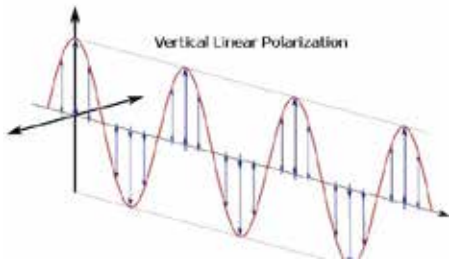


Fig. 19. The total (0.325–4.6 μm) upward, downward, and net flux profiles near the Venera 11 and 12 entry sites ($\theta_s = 19.3^\circ$).



Polarization of sunlight reflected by Venus



Hansen & Hovenier (1974)

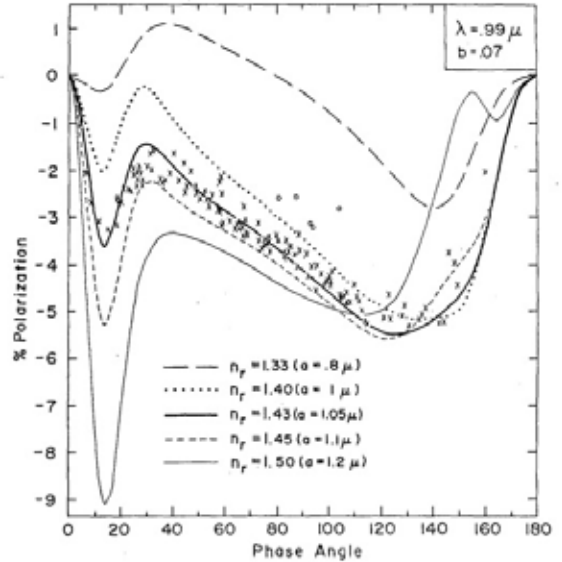


Fig. 7. Observations and theoretical computations of the polarisation of sunlight reflected by Venus at $\lambda = 0.99 \mu$. The observations were made with an intermediate bandwidth filter, the 'x's being obtained by Coffeen and Gehrels (1969) in 1959-67 and by Coffeen (cf. Dollfus and Coffeen, 1970) from 1967 to March 1969, and the 'o's being obtained by Coffeen (cf. Dollfus and Coffeen, 1970) in May-July, 1969. The theoretical curves are for spherical particles having the size distribution (8) with $b = 0.07$. The different theoretical curves are for various refractive indices, the effective particle radius being selected in each case to yield closest agreement with the observations for all wavelengths.

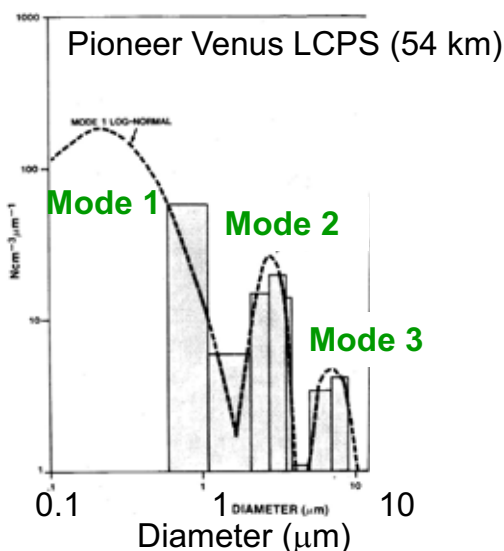
Refractive index = 1.44

→ consistent with $H_2SO_4-H_2O$ solution

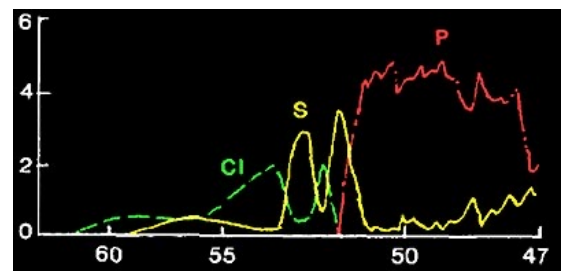
Effective radius $\sim 1 \mu m$

Microphysical properties of Venus clouds

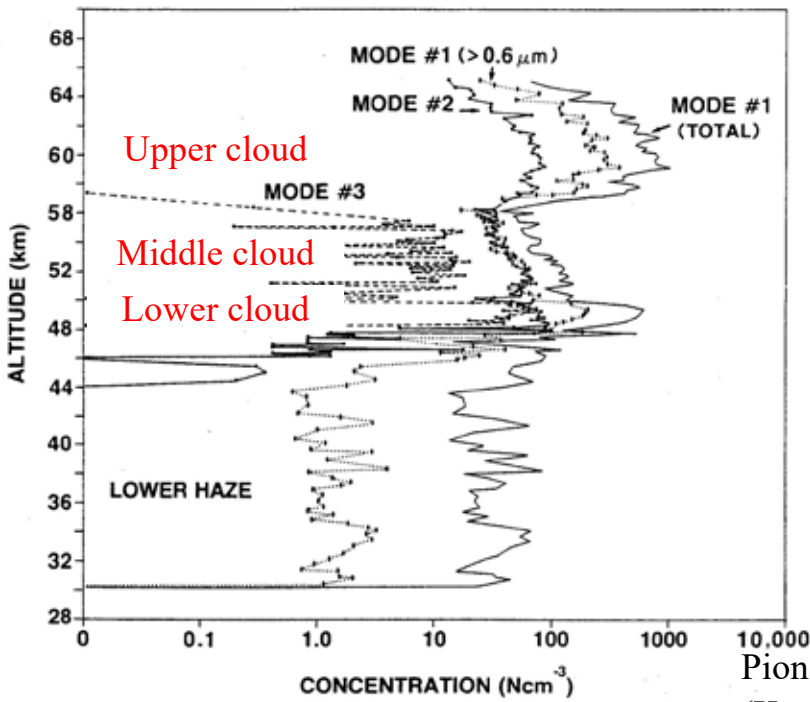
- $H_2SO_4-H_2O$ droplets with radii $r < 5 \mu m$
- Smallest mode (including sub-cloud haze) might be condensation nuclei whose composition is unknown.
- Size distribution is variable.



Venera-13 Lander



Three-layered structure of Venusian clouds

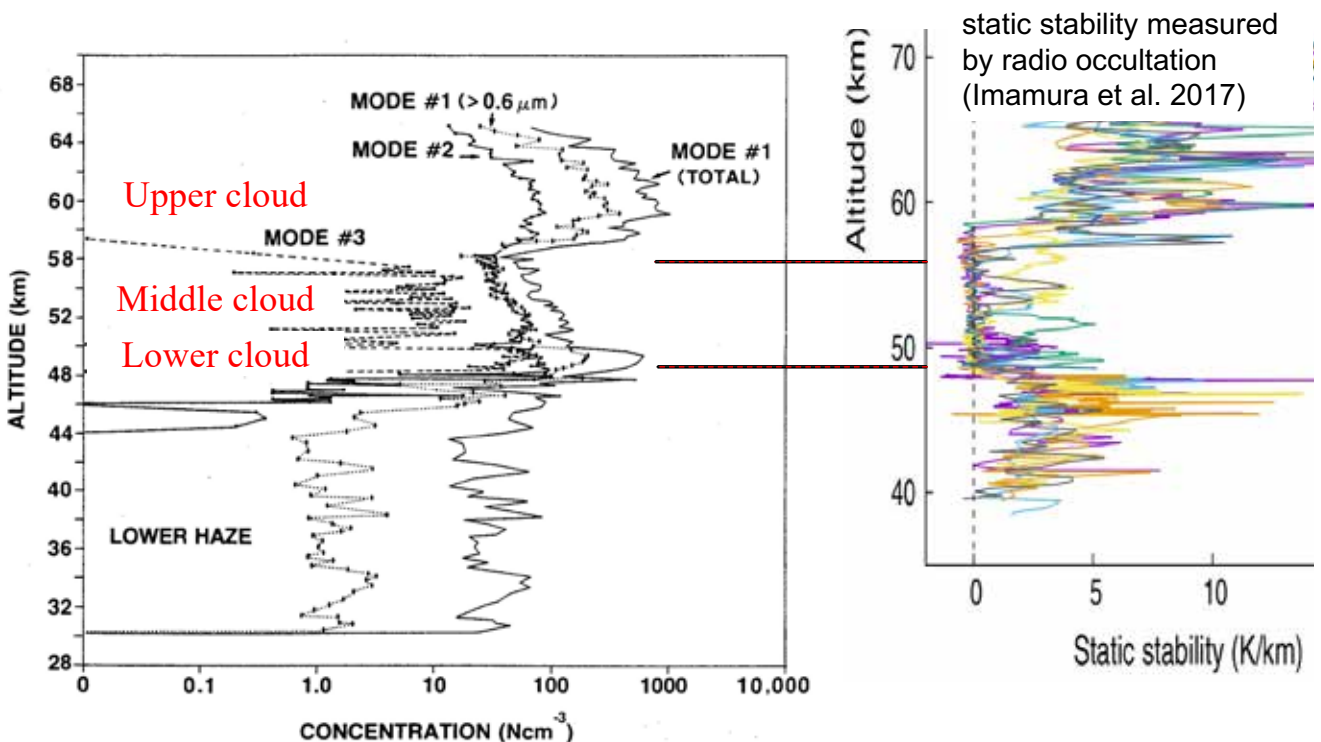


Pioneer Venus LCPS
(Knollenberg and Hunten, 1980)

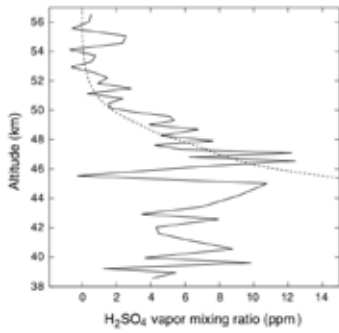
The bulk of the mass exists in Mode 2 ($r \sim 1 \mu\text{m}$)

The bulk of the mass exists in Mode 2 and 3 ($r = 1\text{-}5 \mu\text{m}$)

Three-layered structure of Venusian clouds



H₂SO₄ vapor in Venusian atmosphere



Imamura et al. (2017)

Measurement by radio occultation

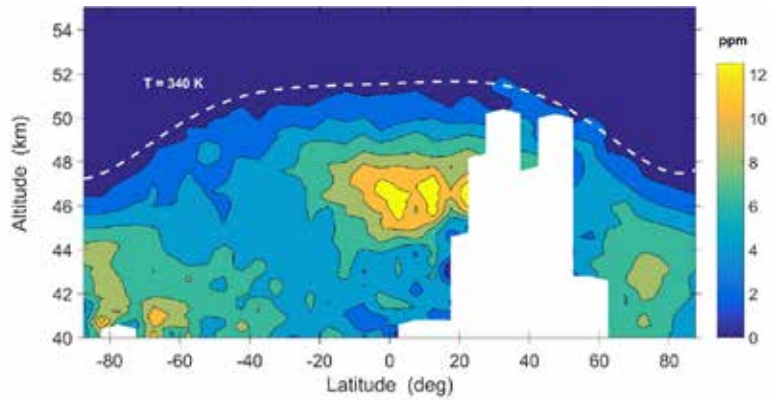


Fig. 9. Zonally and time-averaged sulfuric acid vapor distribution in the Venus lower atmosphere at all latitudes between the years 2006 and 2014 (lower panel). The hemispheres were subdivided into equal latitudinal bins of 5° each and H₂SO₄(g) profiles located within each bin were averaged to one mean profile. The number of data samples used for averaging is shown in the upper panel. The white dashed line in the lower panel shows the isotherm at T = 340 K derived from VeRa X-band radio occultation data from the same period. The H₂SO₄(g) values above this isotherm are generally as high as their uncertainties. Below the isotherm the values are higher than their uncertainties. The lack of measurements at northern mid latitudes between 20° and 60° is a consequence of the VEX orbit geometry.

Oschlisniok et al. (2021)

Sulfur-rich atmosphere: origin of H₂SO₄

SO₂ measurements by Vega landers

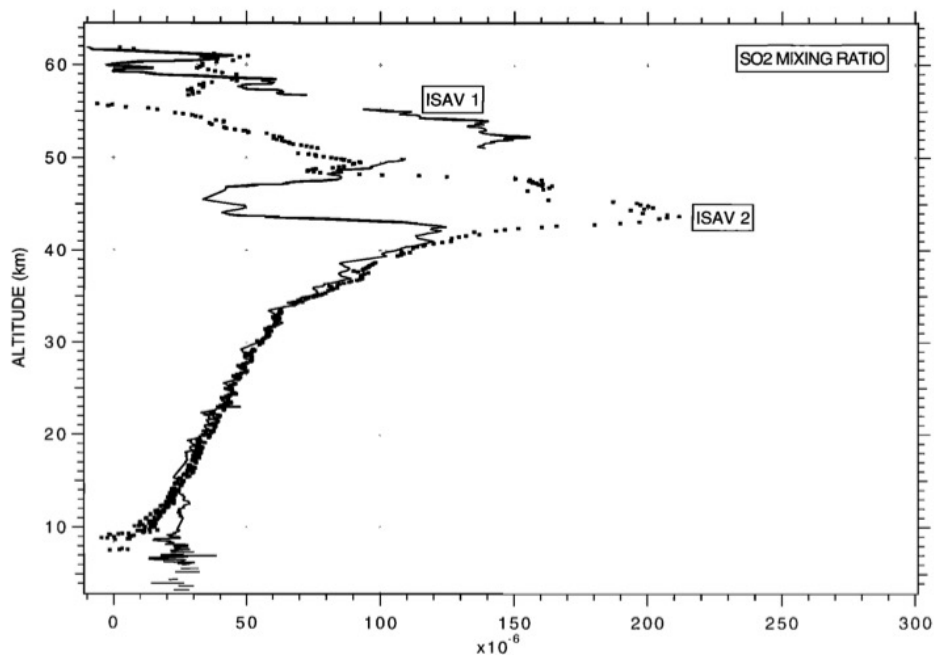
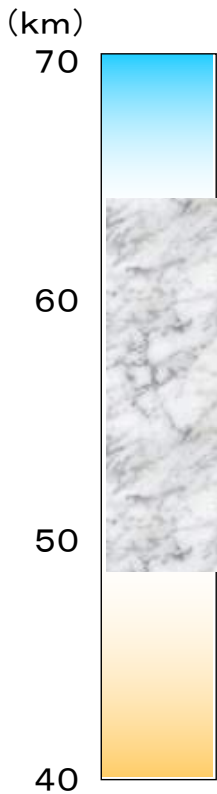


Figure 24. The SO₂ mixing ratio vertical profile retrieved for ISAV 2 (data points) is compared to that determined for ISAV 1. There is a large difference of structure above 40 km, while the profiles are nearly identical below 40 km. A peak of 210 ppm is observed at 43 km in the ISAV 2 data.

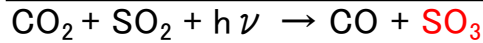
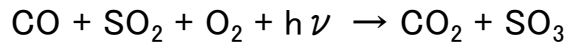
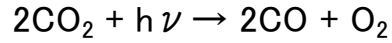
Bertaux et al. (1996)

Origin of clouds

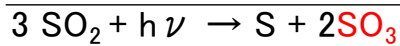
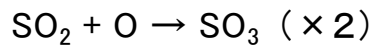
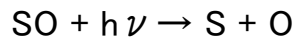
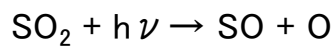


Photochemistry above clouds

Scenario #1 (Net reaction driven by catalytic cycles including ClO_x, HO_x, NO_x)



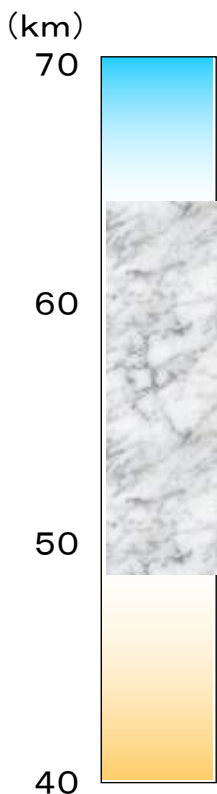
Scenario #2



▪ SO₃ rapidly reacts with H₂O: $\text{SO}_3 + \text{H}_2\text{O} \rightarrow \text{H}_2\text{SO}_4$

▪ Elemental sulfur (S) can serve as condensation nuclei.

Origin of clouds

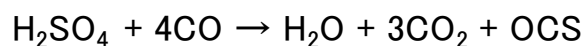
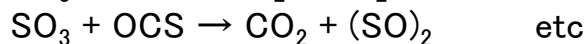
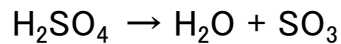


H₂SO₄ vapor and H₂O vapor condenses onto condensation nuclei.

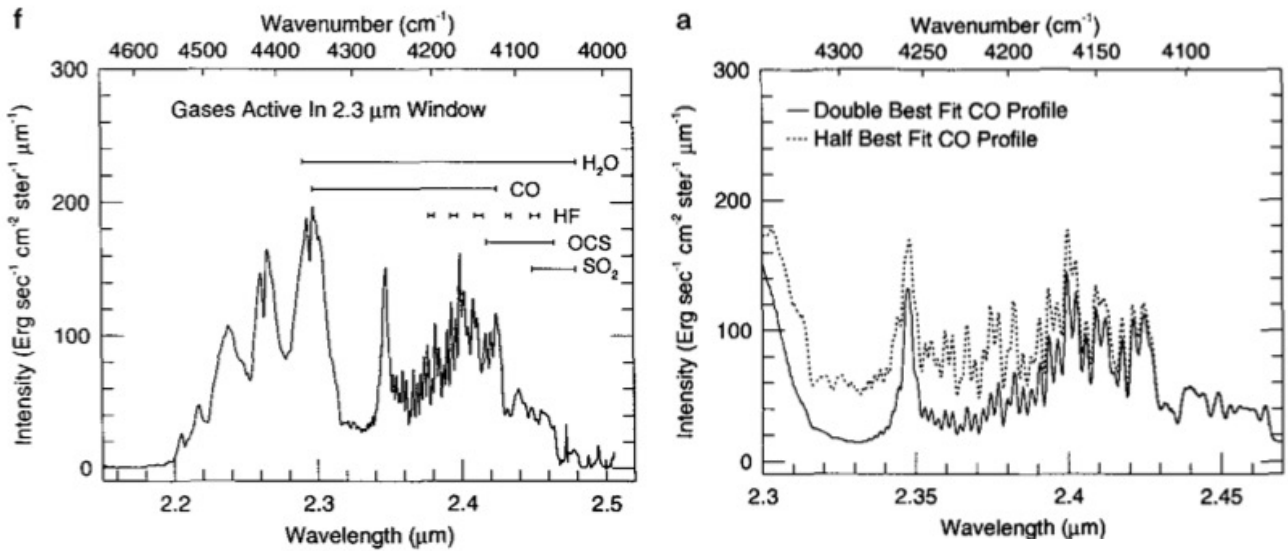
Growth of particles via collision during gravitational sedimentation

Evaporation around 50 km altitude due to high temperature

Thermochemistry below clouds (Net reaction driven by catalytic cycles)

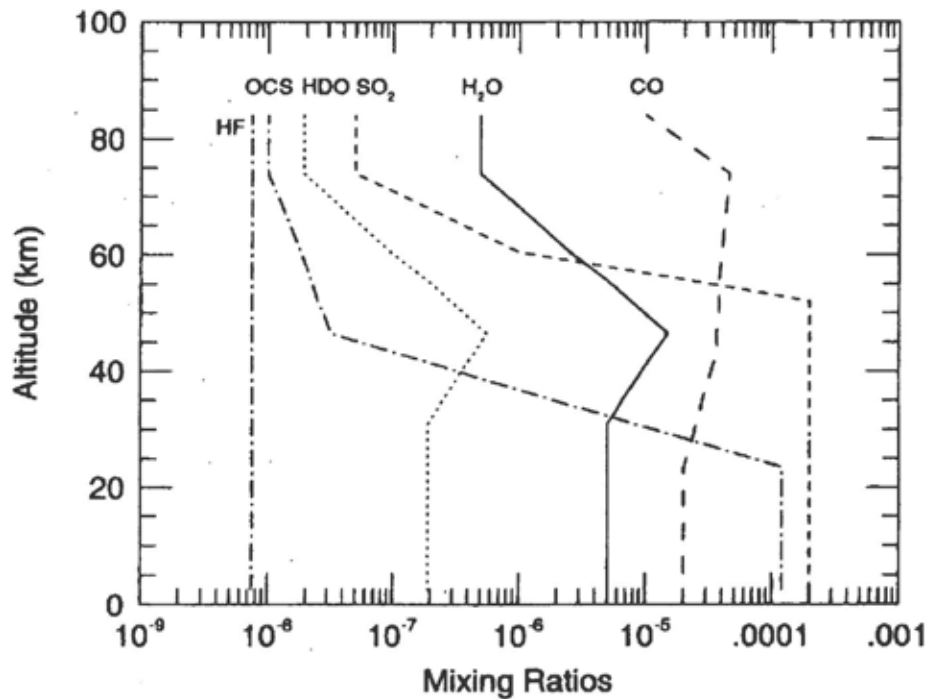


Ground-based observations of cloud-related gaseous species



Pollack et al., Icarus 103, 1, 1993

Retrieved vertical profiles



Pollack et al., Icarus 103, 1, 1993

Sedimentation of particles

Stokes velocity for a spherical particle

$$w_{\text{sed}} = \frac{g\rho d^2}{18\eta}$$

- g : gravitational acceleration
- ρ : mass density of particle
- d : diameter of particle
- η : viscosity coefficient of air

comparable 

Time constant of Hadley circulation
 $\tau \sim 100$ Earth days (from energy budget)
 \rightarrow Vertical flow velocity $\sim H/\tau \sim 1$ mm/s

Sedimentation velocity of droplets in
 Venusian atmosphere
 (Imamura & Hashimoto 1998)

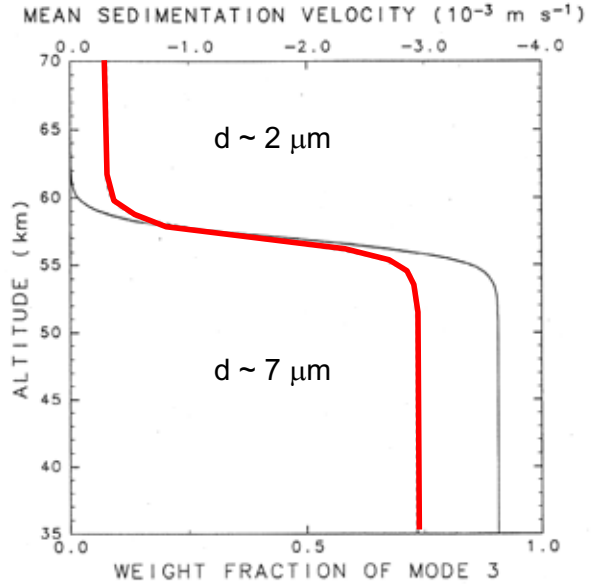
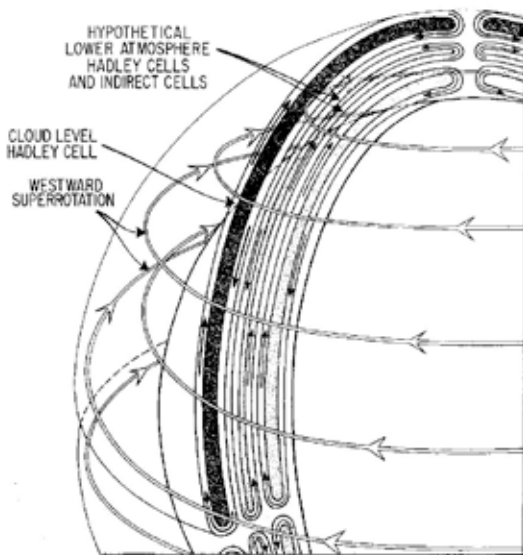
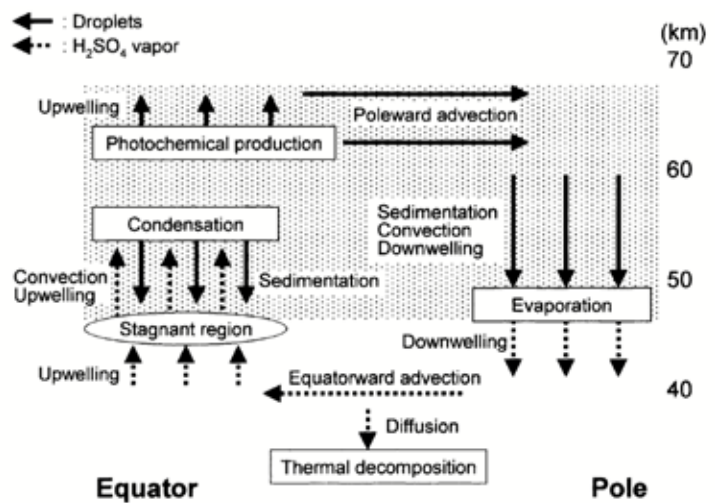


Figure 2. Fraction of Mode 3 particles by weight in the cloud (solid curve) adopted in the model after the observation by the Pioneer Venus particle size spectrometer, and the calculated mean sedimentation velocity W_{sed} (dashed curve). The cloud mass is assumed to be composed of particles of fixed radii, Mode 2 ($r = 1.15 \mu\text{m}$) and Mode 3 ($r = 3.65 \mu\text{m}$).

Possible role of planetary-scale meridional circulation

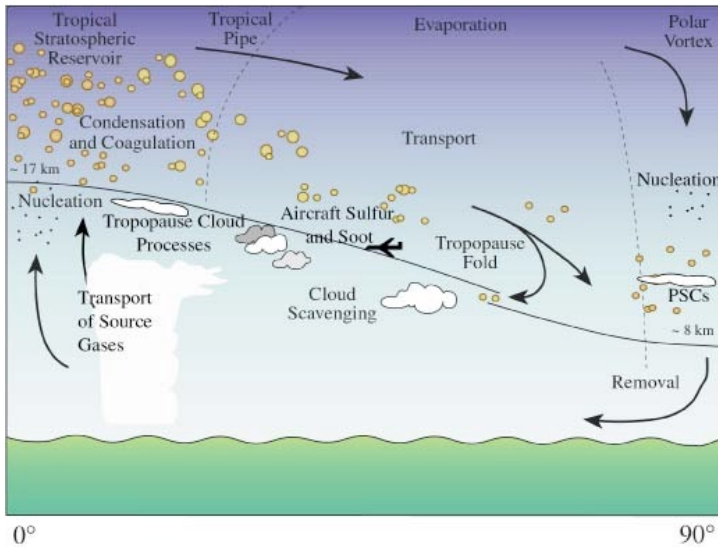


Schubert (1983)



Imamura & Hashimoto (2001)

Lifecycle of Earth's stratospheric aerosols



Hamill et al. (1997)

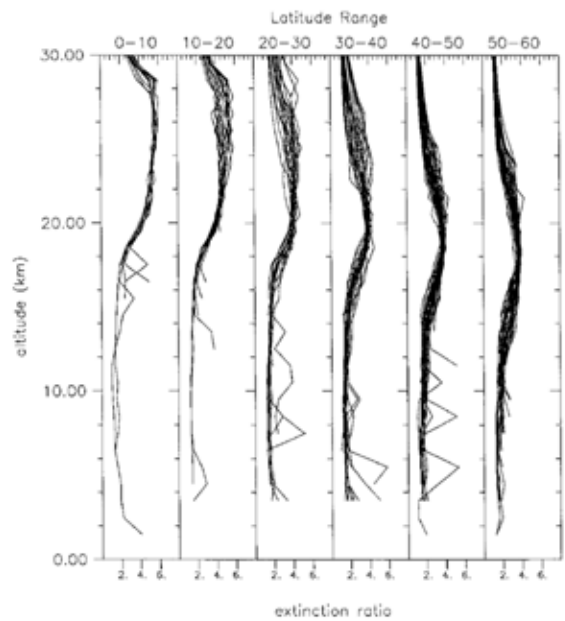
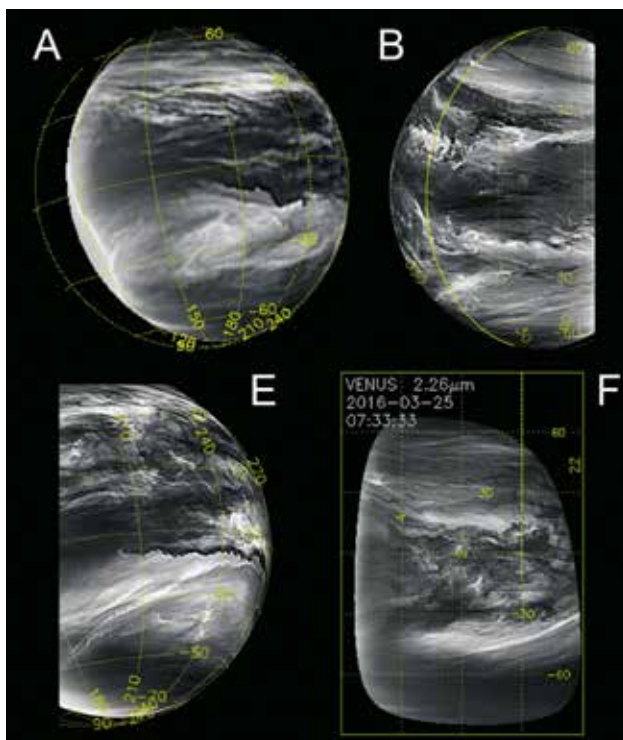


FIG. 9. Extinction ratios from the SAGE II satellite system in various latitude ranges. The extinction values were measured in April 1989 in the Southern Hemisphere. We have removed extinction ratios greater than 7 at lower altitudes for these are indications of tropospheric clouds.



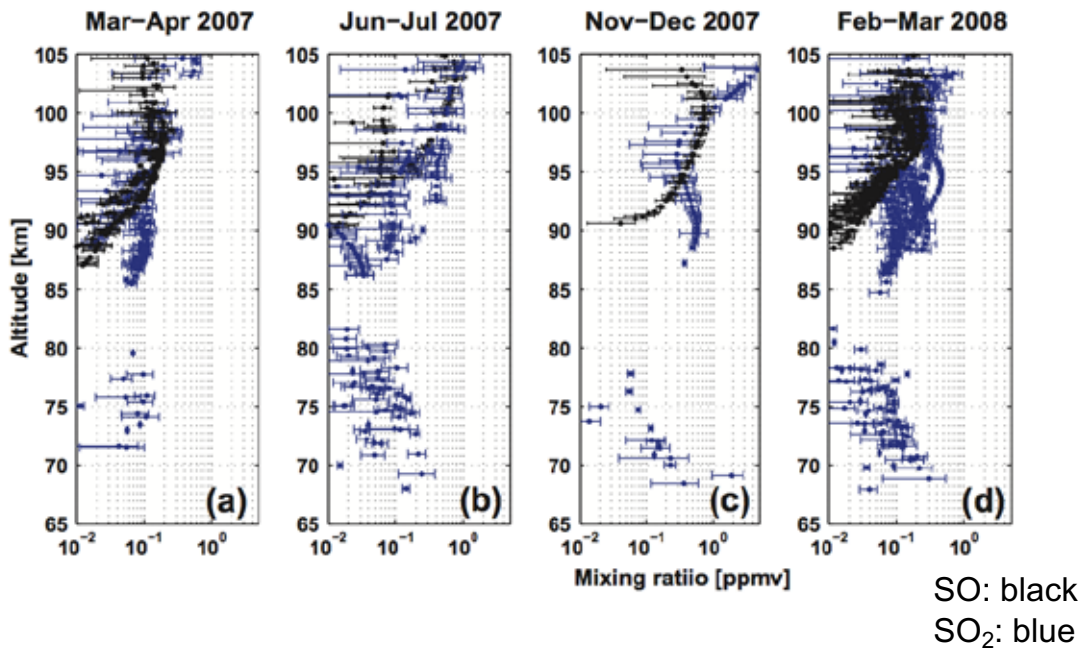
Observed cloud morphology



Peralta et al. (2018)

Equatorial dark clouds might be produced by large-scale upwelling near the cloud base

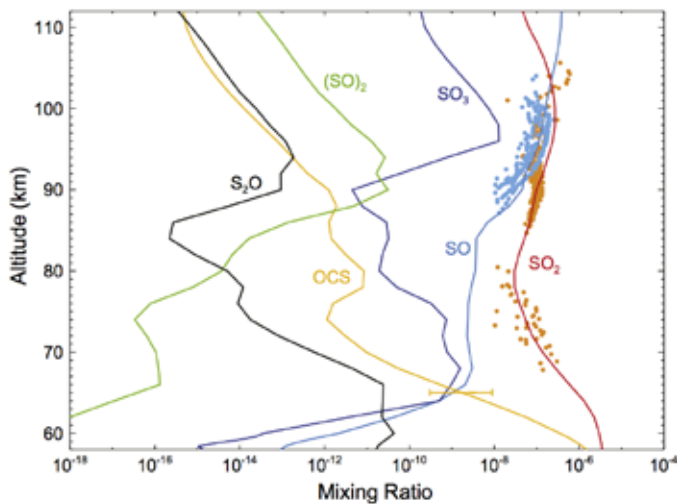
SO, SO₂ profiles above cloud observed by Venus Express solar occultations (Belyaev et al. 2011)



- Enhancement at high altitudes cannot be explained by traditional photochemical models.

Chemical model of Venusian stratosphere (Zhang et al. 2012)

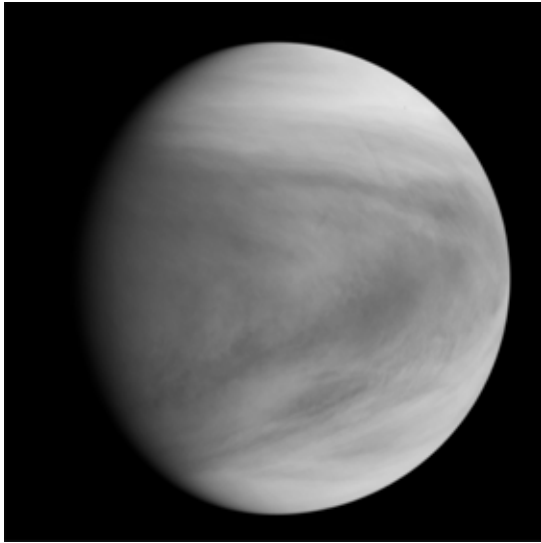
Artificial H₂SO₄ source added above 90 km:



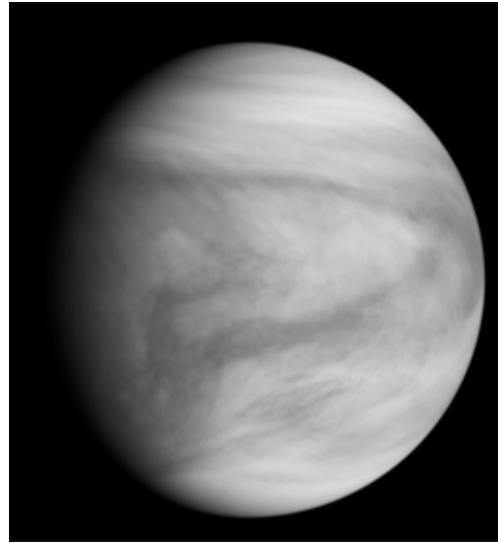
Transport of cloud particles to the upper atmosphere by winds ?
→ Open question

Fig. 8. Same as Fig. 2, for the sulfur oxides. The SO₂ and SO observations with errorbars are from the Belyaev et al. (2012). The temperature at 100 km is 165–170 K for the observations. The OCS measurement (0.3–9 ppb with the mean value of 3 ppb) is from Krasnopolsky (2010).

SO₂ (283 nm)



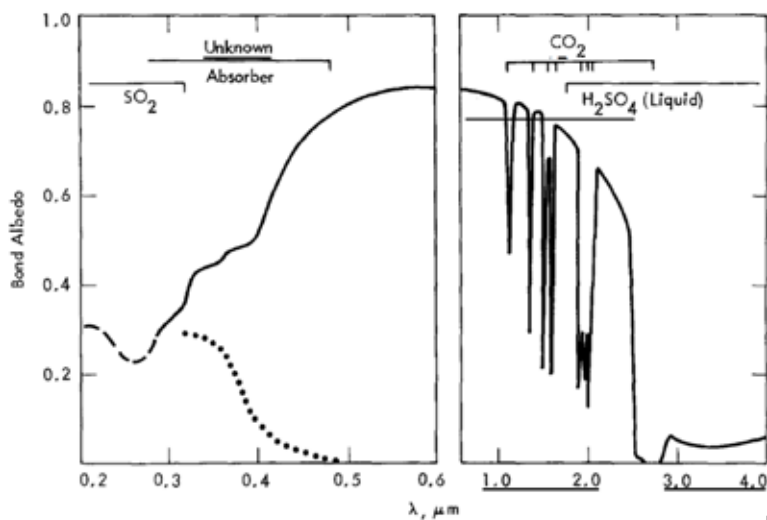
Unknown absorber (365 nm)



Venus is completely covered by clouds that are featureless in the visible but exhibit variable ultraviolet features.

Origin of visible-UV absorption

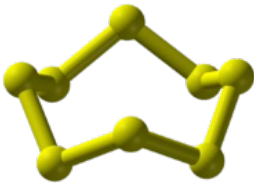
- Absorbing material at far UV (<320nm) is mostly SO₂
- Absorption at near UV (>320nm) is a mystery. Candidate species are S, S₂O₂, S₂O, FeCl₂, etc.



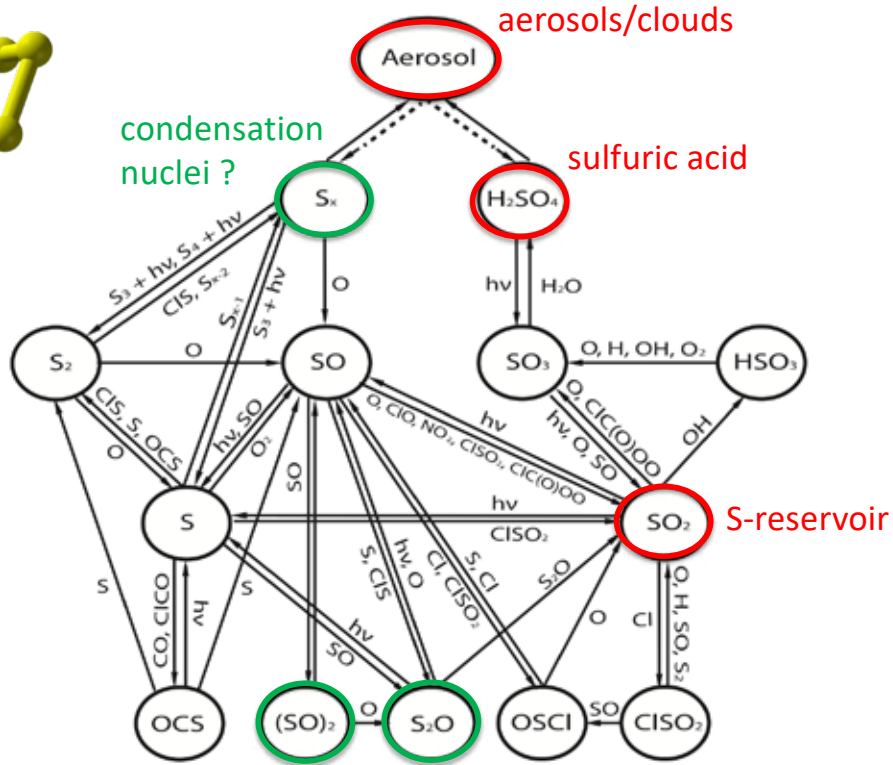
Moroz et al. (1985)

Figure 6-1. The Monochromatic Bond Albedo of Venus as a Function of Wavelength (Moroz, 1983 - Normalized to the Integrated Albedo $A = 0.76$). The points show the wavelength dependence of the maximum contrast between dark and light UV features (Coffeen, 1977).

Sulfur cycle in Venus's atmosphere

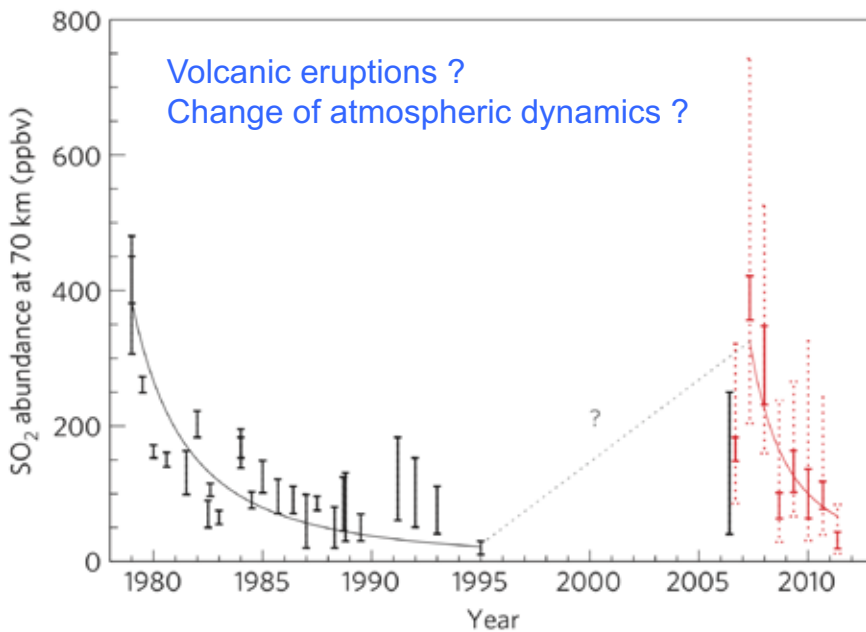


S₈



Zhang et al. (2012)

Variability of SO₂ above clouds



Marcq et al. (2013)

Figure 3 | More than thirty years of SO₂ measurements at Venus's cloud top. Black stands for previously published measurements²⁶. Red stands for the 8-month moving average of the retrievals also shown in Fig. 1. Solid red error bars represent 1 σ random uncertainty, and dotted red error bars represent measurement dispersion in each temporal bin.